



## Article

# Impact of Snowpack on the Land Surface Phenology in the Tianshan Mountains, Central Asia

Tao Yang <sup>1</sup>, Qian Li <sup>2,3</sup>, Qiang Zou <sup>1</sup>, Rafiq Hamdi <sup>4</sup> , Fengqi Cui <sup>5</sup> and Lanhai Li <sup>2,3,6,\*</sup>

<sup>1</sup> Key Laboratory of Mountain Hazards and Surface Process, Institute of Mountain Hazards and Environment, Chinese Academy of Sciences, Chengdu 610041, China; yangtao@imde.ac.cn (T.Y.); zouqiang@imde.ac.cn (Q.Z.)

<sup>2</sup> State Key Laboratory of Desert and Oasis Ecology, Xinjiang Institute of Ecology and Geography, Chinese Academy of Sciences, Urumqi 830011, China; liqian@ms.xjb.ac.cn

<sup>3</sup> Ili Station for Watershed Ecosystem Research, Chinese Academy of Sciences, Yili 835800, China

<sup>4</sup> Meteorological and Climatological Research Department, Royal Meteorological Institute, 1180 Brussels, Belgium; rafiq.hamdi@meteo.be

<sup>5</sup> Department of Geography, Ghent University, 9000 Ghent, Belgium; fengqi.cui@ugent.be

<sup>6</sup> CAS Research Centre for Ecology and Environment of Central Asia, Urumqi 830011, China

\* Correspondence: lilh@ms.xjb.ac.cn; Tel.: +86-991-782-3125

**Abstract:** The accumulation and ablation processes of seasonal snow significantly affect the land surface phenology in a mountainous ecosystem. However, the ability of snow to regulate the alpine land surface phenology in the arid regions is not well described in the context of climate change. The impact of snowpack changes on land surface phenology and its driving factors were investigated in the Tianshan Mountains using the land surface phenology metrics derived from satellited products and a snow dataset from downscaled regional climate model simulations covering the period from 1983 to 2015. The results demonstrated that the annual mean start of growing season (SOS) and length of growing season (LOS) experienced a significant ( $p < 0.05$ ) decrease and increase with a rate of  $-2.45$  days/decade and  $2.98$  days/decade, respectively. The significantly advanced SOS and increased LOS were mainly seen in the Western Tianshan Mountains and Ili Valley regions with elevations from 2500 to 3500 m a.s.l and below 3000 m a.s.l, respectively. During the early spring, the significant decline in snow cover fraction (SCF) could advance the SOS. In contrast, snowmelt amount and annual maximum snow water equivalent (SWE) have an almost equally substantial positive correlation with annual maximum vegetation greenness. In particular, the SOS of grassland was the most sensitive to variations of snow cover fraction during early spring than that of other vegetation types, and their strong relationship was mainly located at elevations from 1500 to 2500 m a.s.l. Its greenness was significantly controlled by the annual maximum snow water equivalent in all elevation bands. Both decreased SCF and increased temperature in the early spring caused a significant advance of the SOS, consequently prolonging the LOS. Meanwhile, more SWE and snowmelt amount could significantly promote vegetation greenness by regulating the soil moisture. The results can improve the understanding of the snow ecosystem services in the alpine regions under climate change.

**Keywords:** snow mass; snow cover fraction; land surface phenology; Tianshan Mountains



**Citation:** Yang, T.; Li, Q.; Zou, Q.; Hamdi, R.; Cui, F.; Li, L. Impact of Snowpack on the Land Surface Phenology in the Tianshan Mountains, Central Asia. *Remote Sens.* **2022**, *14*, 3462. <https://doi.org/10.3390/rs14143462>

Academic Editors: Xiaohua Hao, Hongyi Li, Xufeng Wang, Xiaoyan Wang, Xiaodong Huang and Jian Bi

Received: 6 June 2022

Accepted: 14 July 2022

Published: 19 July 2022

**Publisher's Note:** MDPI stays neutral with regard to jurisdictional claims in published maps and institutional affiliations.



**Copyright:** © 2022 by the authors. Licensee MDPI, Basel, Switzerland. This article is an open access article distributed under the terms and conditions of the Creative Commons Attribution (CC BY) license (<https://creativecommons.org/licenses/by/4.0/>).

## 1. Introduction

Vegetation has a critical effect on Earth's ecosystem, water–heat exchange, and carbon cycles [1–3]. The variability of land surface phenology (the start of growing season (SOS), the end of growing season (EOS), and the length of growing season (LOS)) are controlled by climatic conditions and partly human activities [4,5]. The alpine environment is vulnerable to climate change, and is facing the warming faster than low-elevation regions [6,7]. A warming climate may increase the amount of energy received by seasonally snow-covered areas [8], benefiting the vegetation greening in the high latitude and altitude

regions [9]. In addition, changes in land surface phenology also have feedback to the climate system through biogeochemical and biogeophysical processes [2]. Therefore, it is essential to investigate the relationships between climate change and the alpine land surface phenology.

Currently, most studies focused on clarifying the relationships between the land surface phenology (or tree ring, vegetation index, etc.) and climate factors (precipitation, temperature, soil moisture, etc.) [10–14]. Moreover, some studies attempted to reveal the snow cover effects on land surface phenology in high-elevation and high-latitude areas [15–19]. For example, except for spring temperature, the snow cover durations and melting days were demonstrated as the important secondary factors of SOS variations for grassland and forest in the Alps using the optical remote sensing products and meteorological datasets from 1992 to 2014 [20]. The advanced SOS in Alaska was attributed to the earlier snowmelt timing due to spring warming based on multiple data sources during 2000–2019 [21]. As an excellent indicator of climate change, the seasonal snowpack is defined as the most sensitive land surface variable to the changes in precipitation and temperature for both time and space [22]. It not only provides the fundamental freshwater for the alpine regions [23,24], but also regulates the climate system and ecosystem service due to the excellent insulating properties and high albedo [22,25,26]. Since snow accumulates during the cold season, an increase in snow depth and longer snow cover duration could prevent vegetation damage from low temperatures and wind in winter [27]. Meanwhile, more snowmelt could replenish the soil moisture in early spring and contribute to vegetation greenness [28]. For example, the winter snow depth could regulate the desert vegetation growth until summer by consistently influencing soil moisture [27,29]. Climate warming could alter snowmelt timing and shorten the snow cover duration [30,31]. The timing of snow accumulation and ablation significantly affects SOS and LOS [16]. However, a relatively short time series of the common snow cover dataset could not fully reveal the inter-annual trends of snow mass and meteorological factors, and their impact on land surface phenology at a landscape level. Additionally, it is a big challenge to accurately estimate the snow mass in the mountainous areas due to a sparse meteorological network and complex underlying surface. Therefore, the response of alpine land surface phenology to the snow changes still requires further research at an interdecadal time scale.

The Tianshan Mountains (TS) are believed to serve as the water towers and ecological barrier of arid Central Asia, providing a large amount of glacier/snow melt water for irrigated agriculture and ecosystem [32,33]. The warming rate in the TS is twice compared with the global average level [34]. Snow cover duration experienced a significant decrease, and snow end date advanced significantly [35,36], but the annual maximum snow storage kept a relatively stable status [37]. Several studies have proved that regional vegetation is sensitive to water deficits, temperature, precipitation, and human activities [38–41]. Meanwhile, a longer snow cover duration could lead to a greater annual maximum normalized difference vegetation index ( $NDVI_{max}$ ) values of pasture in the Western TS [17]. However, the response of land surface phenology to the snowpack changes (snow cover fraction, snow mass, and snow depth, etc.) cannot be adequately revealed by MODIS snow cover due to the limitation of optical sensor [28,42], and its driving mechanisms need to be better explored in the entire TS. In addition, the accuracy and coarse resolution of the existing snow mass datasets also bring a big challenge for finer-scale snow ecology research [43].

This study aims to investigate the influence of snow characteristics changes on land surface phenology and clarify the driving mechanisms in the TS using the land surface phenology metrics derived from satellited products and a snow dataset from the Weather Research and Forecasting model (WRF) downscaled simulations spanning the period from 1983 to 2015. The specific objectives are as follows: (1) to investigate the spatiotemporal variability of land surface phenology (SOS, LOS, and  $NDVI_{max}$ ) and related snow metrics (snow cover fraction (SCF), annual maximum snow water equivalent ( $SWE_{max}$ ), and snowmelt amount); and (2) to explore the relationships between snow changes and vegetation dynamic. This is the first attempt to reveal how the snow changes modulate land

surface phenology in the entire TS. The results of this study will improve our understanding of snow ecosystem service.

## 2. Data and Methods

### 2.1. Study Area

The TS are the largest mountain system of Central Asia (Figure 1a), spanning from Xinjiang (China), southeastern Kazakhstan and Uzbekistan to Kyrgyzstan. They have a length of approximately 2500 km and measure a width of 250–350 km, and the average altitude is close to 4000 m above sea level (a.s.l.). The TS are geographically divided into four parts: (1) the Western Tianshan Mountains (WTS), (2) the Northern Tianshan Mountains (NTS), (3) the Eastern Tianshan Mountains (ETS), and (4) the Southern Tianshan Mountains (STS) [44]. Affected by the westerlies and the terrain obstruction, the TS exhibit a distinct continentality gradient with an increasing temperature and precipitation from southeast to northwest. The annual total precipitation and mean temperature amount to 329.3 mm and 4.6 °C, respectively [35]. The annual total precipitation exceeds 500 mm along the northern slope of the TS and the WTS, but amounts are below 100 mm around the Tarim Basin [45]. The precipitation in the ETS and NTS mainly occurs in spring and early summer, which is earlier than that in the STS (summer) but later than the WTS (later winter to early spring) [44]. The abundant precipitation in the mountainous regions forms a “wet island” in the arid land and benefits to shape the richly glaciated and snow-covered areas [44,46], which provides the freshwater for the mountain-oasis-desert ecosystem [33]. In addition, the annual maximum snow mass storage and mean snowfall in the TS reaches about 97.85 gigatons and 84.53 mm, respectively [37,47]. The TS exhibit a rich vegetation diversity ecosystem (Figure 1b), and grassland is the dominant land cover type (Figure 1c).

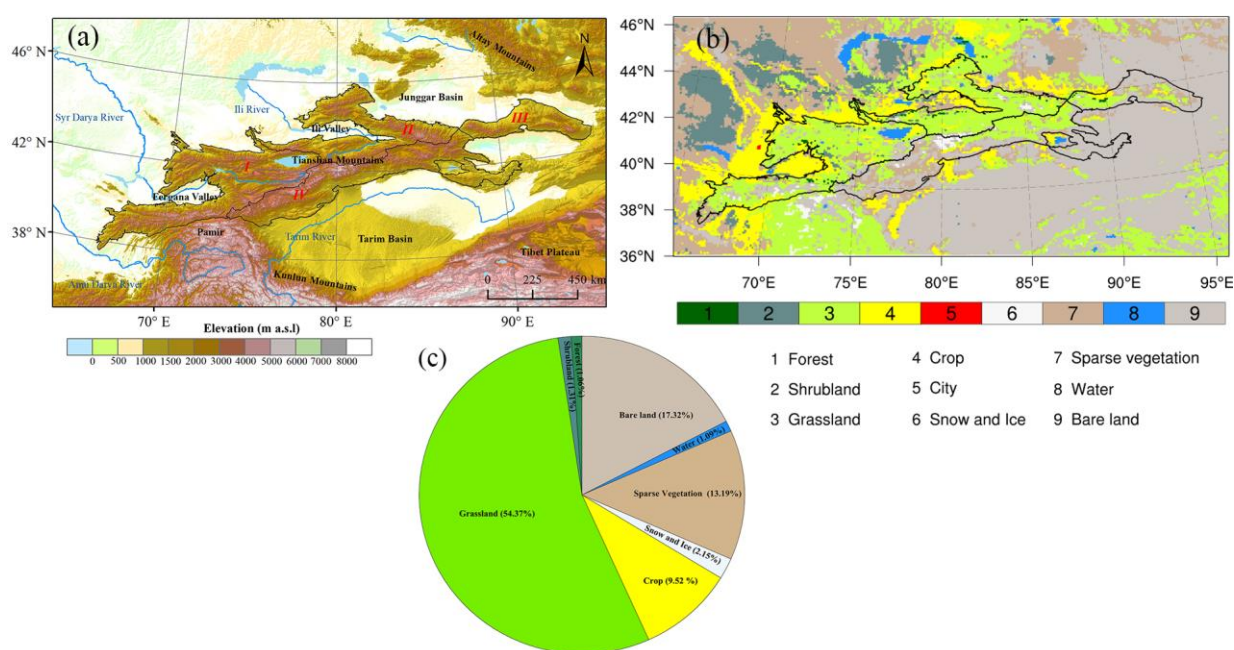


**Figure 1.** (a) Topography (m), (b) land cover type (conversion from basis land over in the WRF second simulation domain), and (c) each type fraction in the Tianshan Mountains.

### 2.2. Datasets

#### 2.2.1. Vegetation Product

Normalized Difference Vegetation Index–3rd generation data from 1983 to 2015 at 8 km spatial resolution, and the 15-day temporal resolution was obtained from the Global Inventory Mapping and Monitoring (GIMMS) group (<https://ecocast.arc.nasa.gov/data/pub/gimms/3g.v1/>, accessed on 20 July 2021). This dataset is generated by Advanced Very-High-Resolution Radiometer (AVHRR) instrument, and underwent a firmly quality

control process before its release [48]. GIMMS NDVI 3g has been widely applied for the long-time trend analysis of vegetation biomass and its phenology dynamics in the Tibet Plateau surrounding areas due to its good temporal consistency and fine quality [48,49]. The land cover type was collected from the European Space Agency (ESA) Climate Change Initiative (CCI) project (<https://www.esa-landcover-cci.org/>, accessed on 20 February 2020), which consists of a series of global land cover maps from 1992 to the present and the overall accuracy exceeds 75.4% [50], and it also exhibited highest overall accuracy in China compared with other six coarse-resolution land cover datasets [51]. In addition, the vegetation parameter has a significant effect on the land surface water–heat process simulation. Thus, to keep the consistency of land cover in the previous land surface simulation and later land surface phenology analysis, the basis land cover was derived from the WRF basis land over (Figure 1b, CCI-LC 2000 map) for further relationship analysis about the phenology from different land covers and the output from WRF model. [37].

### 2.2.2. Climate Data

The daily gridded SCF, SWE, surface air temperature (T<sub>2</sub>), surface albedo, snowmelt amount, and soil moisture content (SMOIS) with a 9 km spatial resolution from 1982 to 2015 were obtained from the outputs of WRF-AWR 4.01 [52] coupled with Noah-MP model [53] one-way double-nested dynamic downscaling simulation, which was forced by 6 h interval ERA5 reanalysis from October 1982 to September 2018. Compared with in situ and remote sensing observations, the snow characteristics, precipitation, and temperature from WRF downscaled simulation showed high accuracy, especially the correlation coefficient of daily snow depth and SWE overall exceeded 0.85 [37]. The detailed physical parameterizations configuration and set up of WRF simulation was shown in [37]. Since the annual maximum snow mass storage in the sub-regions of TS occur in February, March, and April (FMA) [37], the snow-related climate metrics during February, March, and April (SCF<sub>FMA</sub>, Snowmelt<sub>FMA</sub>, T<sub>FMA</sub>, SMOIS<sub>FMA</sub>, and Albedo<sub>FMA</sub>) were chosen to analyze the snow effect on early spring land surface phenology.

### 2.3. Land Surface Phenology Method

The thresholds methods and change detection methods were widely applied to estimate land surface phenology metrics [54]. Previous studies demonstrated that the dynamic threshold method is simple and could effectively derive land surface phenology metrics in Central Asia and Tibet Plateau [41]. Considering the validation data are still scarce in the TS, the NDVI<sub>ratio</sub> of 20% has a good accuracy in SOS estimation in surrounding regions of the TS [41] and the EOS was determined by NDVI<sub>ratio</sub> of 60% in Tibet Plateau [55,56], which has a similar land cover and alpine environment. Therefore, the dynamic thresholds method (NDVI<sub>ratio</sub> of 20% and 60%) was used to determine the SOS and EOS, respectively [57,58]. The 15-day NDVI data were interpolated to a daily time scale, and the Savitzky Golay filter was used to smooth out the noise of the NDVI time series [59]. The NDVI<sub>ratio</sub> could be calculated as:

$$\text{NDVI}_{\text{ratio}} = \frac{\text{NDVI}_t - \text{NDVI}_{\text{min}}}{\text{NDVI}_{\text{max}} - \text{NDVI}_{\text{min}}} \quad (1)$$

where NDVI<sub>t</sub> represents the NDVI value at the time step t (Day of year, DOY), and NDVI<sub>min</sub> and NDVI<sub>max</sub> demonstrate the minimum and maximum NDVI values in a year, respectively. The length of LOS is equal to EOS minus SOS. In addition, the annual mean NDVI value (1983–2015) < 0.1 was used to exclude the background values (bare land) from sparse vegetation (Figure 1b) [60]. The GIMMS NDVI3g product was regridded to a 9 km spatial resolution in order to have the same spatial resolution with WRF outputs before land surface phenology calculation.

### 2.4. Statistical Analyses

The trend magnitudes of land surface phenology and climate factors, and their significant levels were estimated by the Sen's method [61] and Mann–Kendall (M-K) trend

test [62,63], respectively. In addition, the relationships between the land surface phenology and climate factors were investigated by the Pearson Correlation coefficient ( $r$ ).

### 3. Result

#### 3.1. Spatiotemporal Distribution of Land Surface Phenology

The annual mean SOS, LOS, and  $NDVI_{max}$  were 106.30 (Day of year, DOY), 162.24 days, and 0.41 in the TS from 1983 to 2015, respectively. The SOS showed an increase from the low-elevation regions to high-elevation regions (Figure 2a), in which the values mainly varied from 70 to 135. In contrast, the LOS exhibited an opposite pattern (Figure 2c), in which a longer growing season was found in the low-elevation region (elevation < 3000 m a.s.l) compared with the high-elevation regions (elevation  $\geq$  3000 m a.s.l). The high  $NDVI_{max}$  values prevailed in the WTS and the low-elevation regions of the Ili Valley, and the corresponding values exceeded 0.6 (Figure 2e).

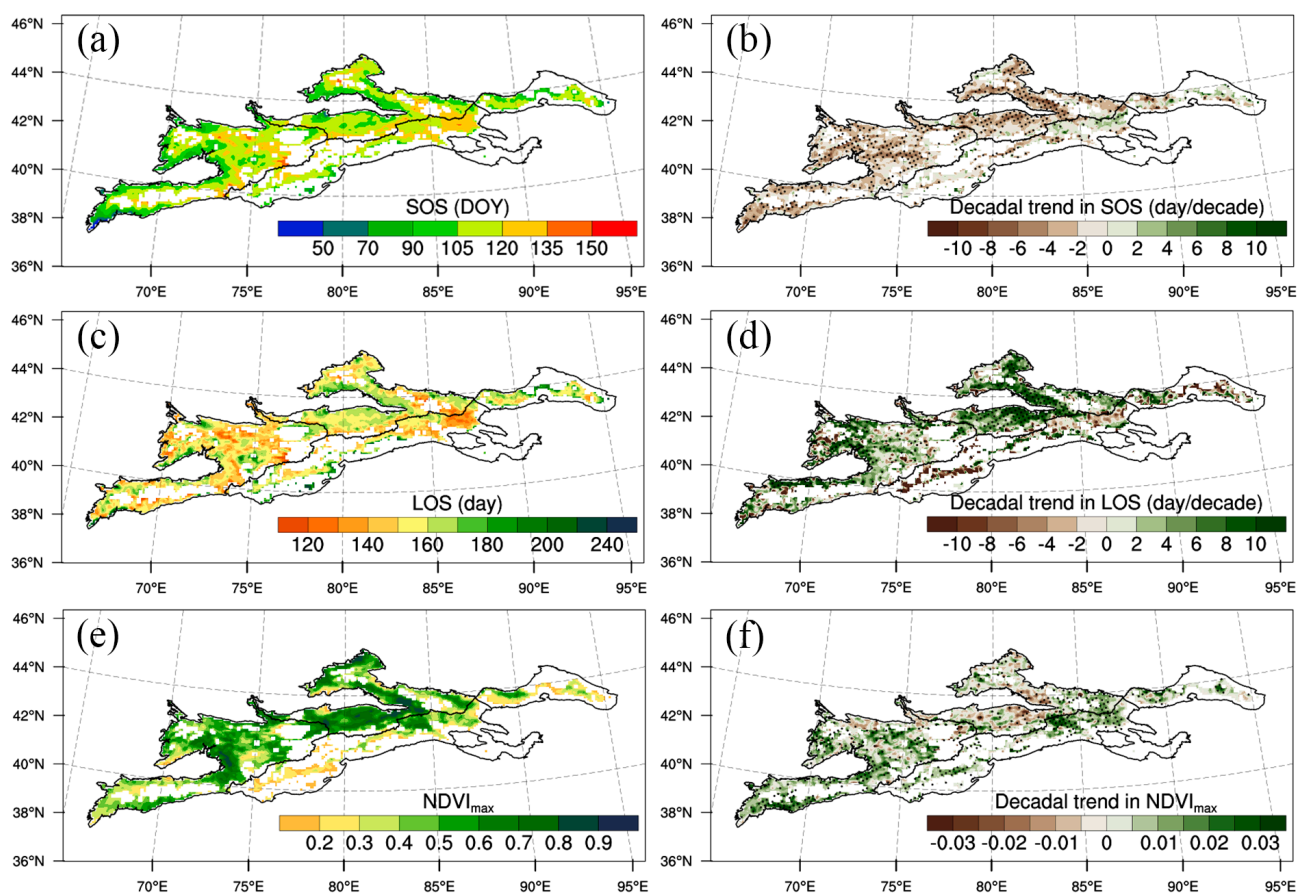


**Figure 2.** Spatial distribution of the mean vegetation metrics (left panels) and their trends (right panels) from 1983 to 2015 (SOS (a) and (b), LOS (c) and (d), and  $NDVI_{max}$  (e) and (f)). The white space in Figure 2 means no data, and the black dots in (b,d,f) indicate the trend at a 0.05 significant level.

The SOS showed a significantly decreasing trend ( $p < 0.05$ ) with a rate of  $-2.45$  days/decade in the TS. The SOS almost exhibited a consistently significant decrease in the entire TS (Figure 2b), especially in the WTS and NTS with an elevation from 2500 to 3500 m a.s.l (Figure 3). The LOS experienced a significant increase ( $p < 0.05$ ) with a rate of 2.98 days/decade. Similarly, most significantly increasing LOS values were noticed in the low-elevation regions of the Ili valley and WTS (Figure 2d), a few significantly decreasing values were found in the low-elevation regions of the northern slope the TS. The  $NDVI_{max}$  showed a slight increase with a rate of 0.004/decade. The significantly increasing  $NDVI_{max}$  values were mainly noticed in the WTS and the intersection of NTS, STS, and ETS (Figure 2f).

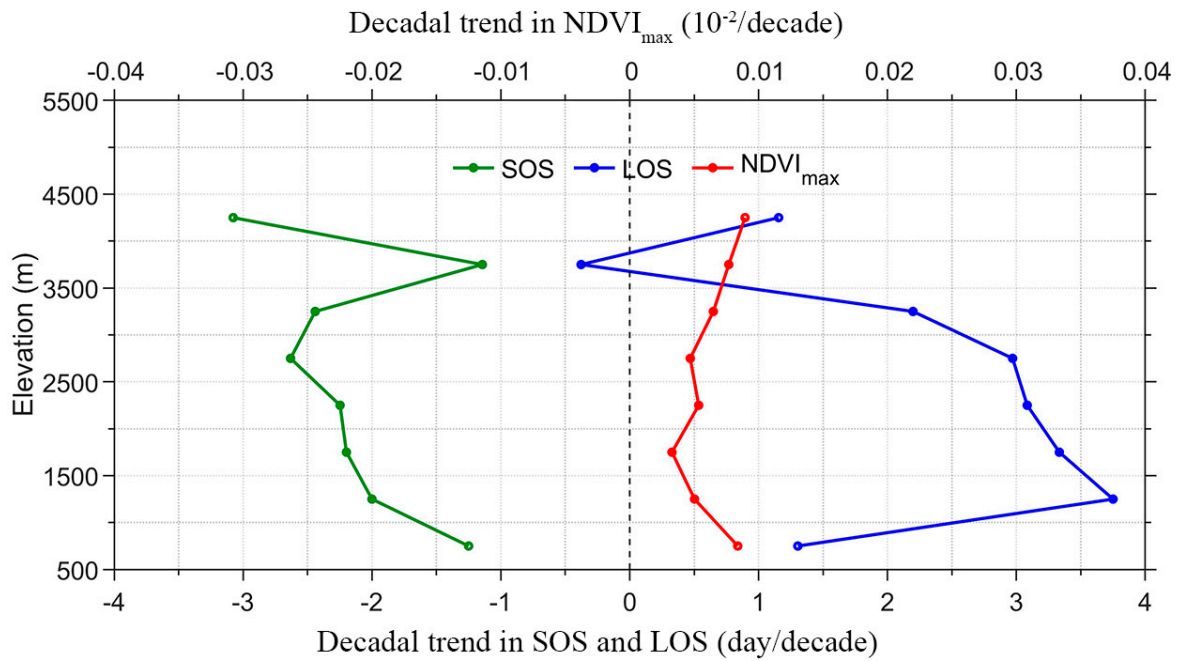


**Figure 3.** Elevation distribution of trend in land surface phenology (SOS, LOS, and  $NDVI_{max}$ ) in the Tianshan Mountains from 1983 to 2015.

3.2. Spatiotemporal Variability of SWE, SCF, and Snowmelt

The variations of SWE, SCF, and snowmelt in the TS are shown in Figure 4. The  $SWE_{max}$  showed a slight increase (with a rate of 2.31 mm/decade in the TS. It exhibited a consistent augmentation in most regions of TS except for the STS (Figure 4a). The significantly increasing values of  $SWE_{max}$  were mainly observed in the ETS. In contrast, the  $SCF_{FMA}$  experienced a slight decline with a rate of  $-1.23\%/decade$ . Almost all regions of the TS showed a consistent decrease (Figure 4b), and a significant decrease in  $SCF_{FMA}$  was seen in the STS. Conversely, the  $Snowmelt_{FMA}$  exhibited a significant augmentation ( $p < 0.05$ ) with a rate of 9.41 mm/decade. The significantly increased values were noticed in the ETS and high-elevation regions of the Ili valley and WTS (Figure 4c), but the decreased values prevailed in the STS.

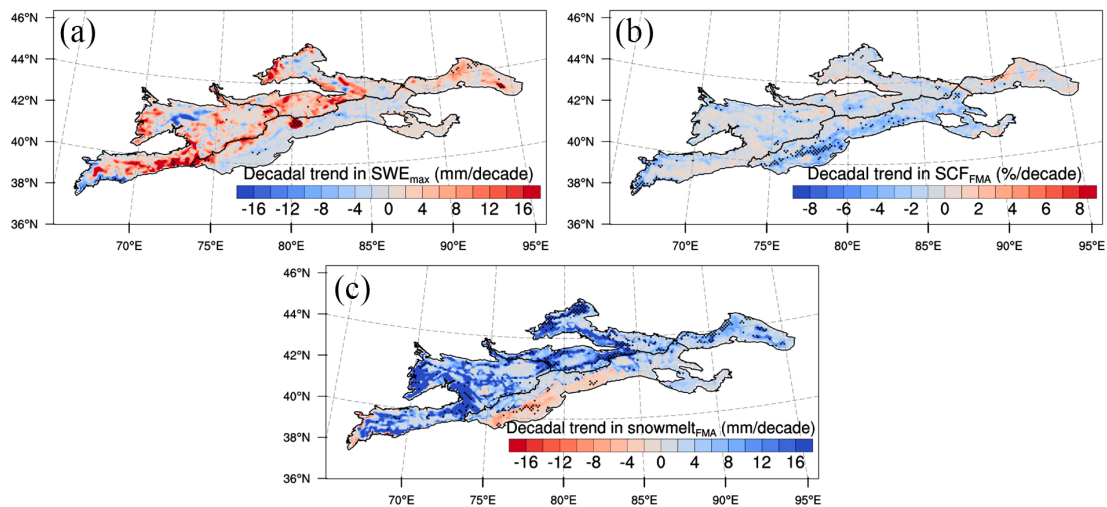


**Figure 4.** Trend distribution of the mean snow metrics:  $SWE_{max}$  (a),  $SCF_{FMA}$  (b), and (c)  $Snowmelt_{FMA}$  from 1983 to 2015. The black dots in Figure 4 indicate the trend at a 0.05 significant level.

### 3.3. Response of Land Surface Phenology to Snow

The relationships between land surface phenology metrics and snow during 1983–2015 are shown in Figure 5. The  $SCF_{FMA}$  had a significant positive effect ( $r = 0.64, p < 0.01$ ) on SOS in the entire TS, especially in the WTS and low-elevation regions of the Ili Valley (Figure 5a). In contrast, the significant positive areas influenced by the  $SWE_{max}$  (Figure 5b) and  $Snowmelt_{FMA}$  (Figure 5c) were smaller and concentrated in the WTS and part low-elevation regions of the intersection of WTS and NTS, respectively. Conversely, the  $Snowmelt_{FMA}$  in the high-elevation regions had a significant negative effect on SOS, particularly in high-elevation regions of the Ili Valley. Compared with a mixed pattern of the relationships between LOS and  $SCF_{FMA}$  or  $Snowmelt_{FMA}$  (Figure 5d,f), the  $SWE_{max}$  had a significant effect on LOS in most regions of TS (Figure 5e). Notably, the  $SCF_{FMA}$  ( $r = 0.36, p < 0.05$ ), the  $SWE_{max}$  ( $r = 0.40, p < 0.05$ ), and  $Snowmelt_{FMA}$  ( $r = 0.44, p < 0.05$ ) showed a significant positive relationship with  $NDVI_{max}$ . All of them exhibited a similar distributional pattern, in which significant positive values were mainly noticed in the WTS and low-elevation regions of the Ili Valley (Figure 5g–i).

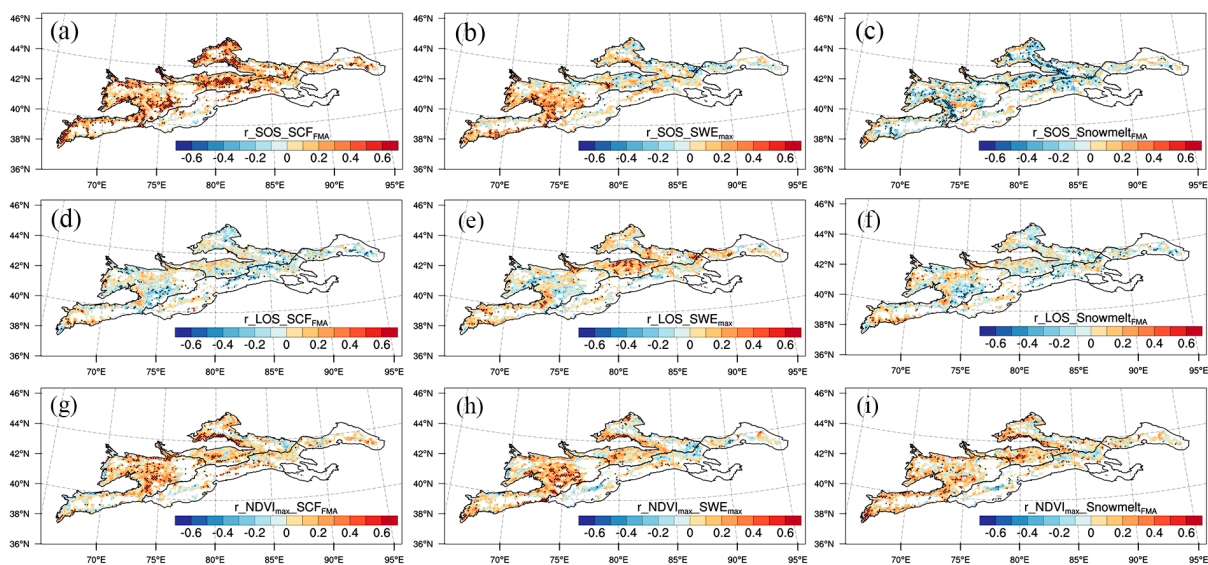


**Figure 5.** Spatial patterns of the correlation coefficient between vegetation metrics and  $SWE_{max}$  (left panels),  $SCF_{FMA}$  (middle panels), and  $Snowmelt_{FMA}$  (right panels) from 1983 to 2015 (SOS (a–c)), LOS (d–f), and  $NDVI_{max}$  (g–i). The white space in Figure 5 means no data, and the black dots in Figure 5 indicate the correlation coefficient at a 0.05 significant level.

## 4. Discussion

### 4.1. Influence of Snow on Land Surface Phenology

The spring land surface phenology is strongly associated with snow cover dynamics in the alpine regions [17,64]. Previous studies suggested that the spring land surface phenology is principally controlled by air temperature [12,65]. Changes in SOS were also primarily influenced by the air temperature during the early spring in the TS (Figure 6), which also confirmed the above views. Meanwhile, the dramatic warming in spring could cause significantly earlier snowmelt dates and the reduction of the  $SCF_{FMA}$  [66], which was recognized as the most ecologically relevant evidence for spring phenology [28,67]. Variation of  $SCF_{FMA}$  has a significant positive effect on the SOS. A significant advanced snow end date and shortened snow cover duration have been reported in the TS due to a warming climate [35,36], which could result in a decrease in  $Albedo_{FMA}$  and feedback to the atmosphere, aggravating warming in spring [68]. Therefore, a decline in  $SCF_{FMA}$  could trigger a widely earlier SOS in the TS due to increases in soil temperature and air temperature during the early spring, especially in the low-elevation regions of the Ili Valley and WTS (Figure 5a), which might contribute to the vegetation germination [69].

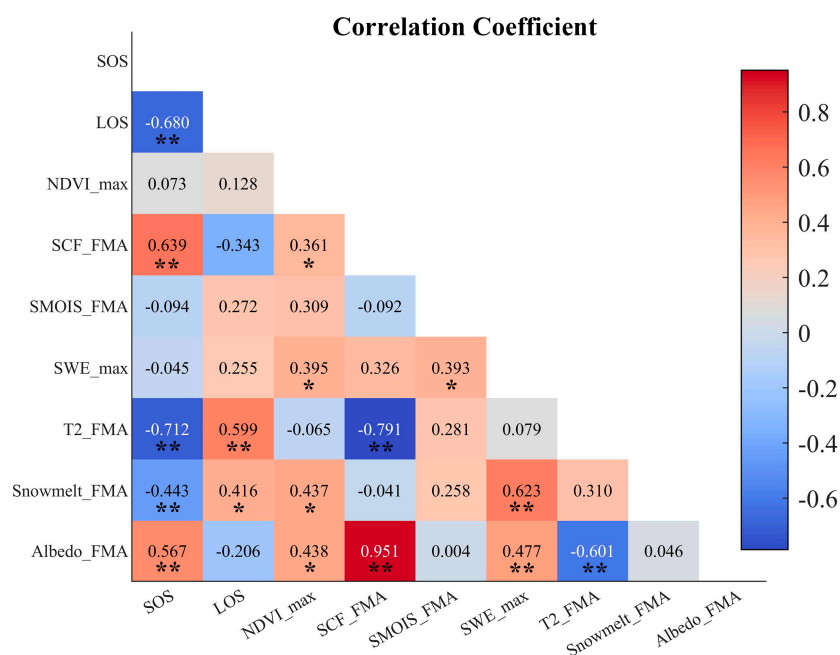


**Figure 6.** Correlation between land surface phenology metrics and climatic factors (\* and \*\* indicate  $p < 0.05$  and  $p < 0.01$ , respectively).

Compared with  $SCF_{FMA}$ ,  $SWE_{max}$ , and  $Snowmelt_{FMA}$  could significantly regulate the annual maximum vegetation greenness in the TS (Figure 6), which could be partly attributed to the interannual variability of temperature and soil moisture during the early growing season [28]. The vegetation growth is limited by water in the low-elevation regions, whereas in alpine and high-latitude regions it is temperature limited [65]. The degree of dependency on snow for vegetation growth is determined by the legacy effect of snow on soil moisture and the demand for moisture conditions during the growing season [28]. Vegetation greenness is greatly sensitive and vulnerable to the water conditions in the TS [38]. A high  $SWE_{max}$  value is always associated with a large snow depth and longer snow cover duration, raising winter soil temperatures and reducing the risk of soil exposure to freezing temperatures [17]. Meanwhile, more  $Snowmelt_{FMA}$  could increase soil moisture contents and promote vegetation greening in the subsequent growing season until the summer [27]. Hence, a widespread significant increase in  $Snowmelt_{FMA}$  is a factor that contributed to a rise in  $NDVI_{max}$ . The wetting and warming tendency might also benefit vegetation greenness in the TS.

#### 4.2. Responses of Different Vegetation Types to Snow

The responses of different vegetation types' phenology to snow dynamics exhibited a distinct difference in the TS, which was consistent with results obtained from other regions such as the Tibetan Plateau and high-elevation regions of the Northern Hemisphere [65,69]. The SOS of grassland was more sensitive to  $SCF_{FMA}$  variations than other vegetation types (Figure 7a). A similar result was also demonstrated in the low-elevation regions of the Ili Valley based on the MODIS snow and vegetation products [42]. Like the Alps [16], the SOS of grassland was influenced primarily by a decline in snow cover, secondarily by snowmelt amount, while the  $NDVI_{max}$  was equally affected by  $SCF_{FMA}$  and  $SWE_{max}$ . Its SOS had a significant positive relationship with  $SCF_{FMA}$ , but a negative relationship with  $Snowmelt_{FMA}$ , indicating that snow plays a vital role in grassland growth onset. This strong positive relationship was mainly located at elevations from 1500 to 3000 m a.s.l (Figure 8a). Notably, although the  $SCF_{FMA}$  was not significant with LOS of grassland, it could significantly affect the LOS below 3000 m a.s.l (Figure 8b). Moreover,  $Snowmelt_{FMA}$  significantly affected the LOS of grassland (Figure 7b), and its greenness was significantly correlated with the  $SWE_{max}$  amount in all elevation bands (Figures 7c and 8c). Overall, the

relations between sparse vegetation and snow variations showed a similar pattern with grassland. The effect of  $SCF_{FMA}$  on LOS of sparse vegetation was more significant than grassland except for elevation below 1000 m a.s.l. Some herb vegetation germination and growth, such as ephemeral plants, heavily depend on the snow conditions around the TS [29]. Large  $SWE_{max}$  and  $Snowmelt_{FMA}$  suggested that snow provided excellent thermal protection and essential moisture supply for shorter plant types [42,56]. Generally, earlier snowmelt with more snowmelt amount could significantly advance the SOS and prolong LOS for grassland, promoting the increase in  $NDVI_{max}$  [16,27]. In contrast, although more  $Snowmelt_{FMA}$  might also replenish the soil moisture, benefit the greenness, and prolong the LOS, earlier snowmelt might restrain the early growth and significantly reduce the  $NDVI_{max}$  for shrubland and forest due to the exposure to the risk of lower soil temperature and wind damage [17,70,71]. It is noted that snow amount could not significantly promote the increase in  $NDVI_{max}$  for forest compared with  $SCF_{FMA}$ , because the air temperatures are more closely correlated with forest than with other vegetation types (Figure 7c) [72]. The main effect of snow on forest growth is to prevent frost damage [73]. The largest precipitation zone in the TS is near the forest line [45], and precipitation is the most important source of soil moisture for later forest growth. In addition, the terrain features (elevation, aspect, and slope) strongly affect alpine species richness, productivity, and nutrient throughout altering the snow metrics dynamics and thermal regime [17,71].

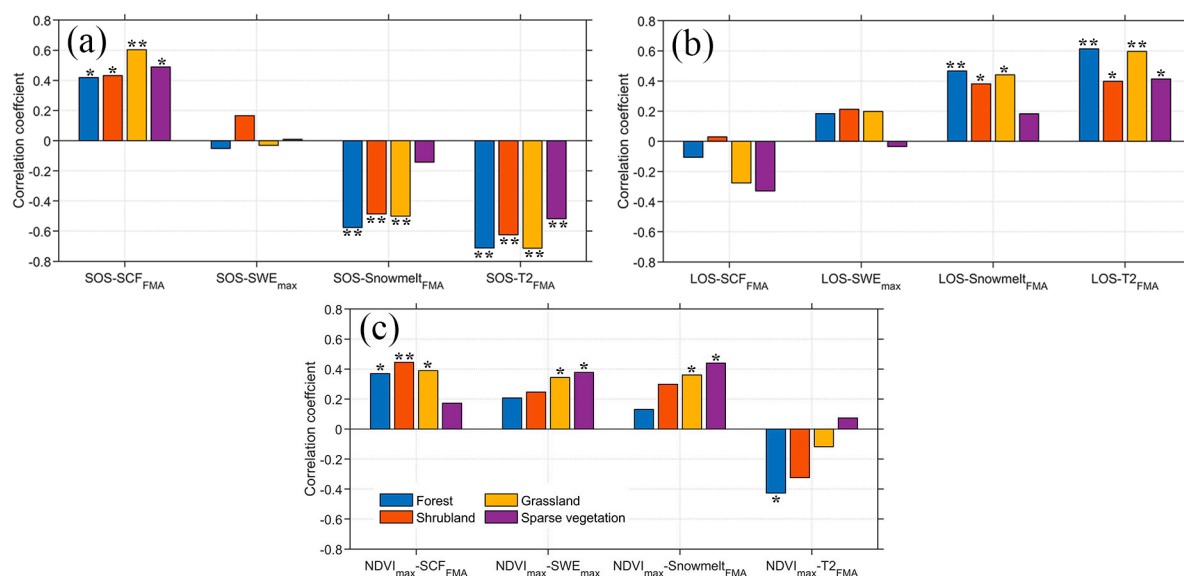


**Figure 7.** Correlation coefficients between (a) SOS, (b) LOS, and (c)  $NDVI_{max}$  and  $SCF_{FMA}$ ,  $SWE_{max}$ ,  $Snowmelt_{FMA}$ , and  $T2_{FMA}$  for each type (\* and \*\* indicate  $p < 0.05$  and  $p < 0.01$ , respectively).

#### 4.3. Limitations and Uncertainties

The performance of the snow dataset generated by a regional model depends on the forcing data accuracy, physical schemes and model parameterizations, and spatial resolution [43,74]. A cold bias, precipitation overestimation, and lack of data assimilation caused a large uncertainty of snow simulation in the high-elevation regions, particularly in the snow ablation period [37,75]. In addition, the spatial heterogeneity of snow could not be revealed in the complex terrains using a relatively coarse resolution (9 km) [76,77]. Similarly, the spatial resolution of GIMMS NDVI 3g is appropriate for landscape-scale research, but maybe not be sufficient for specific species or plant communities at a finer scale [17,78]. The synergistic analysis from the higher remote sensing data (such as MODIS, Landsat, Sentinel-2, Gaofen, and digital cameras) may provide a feasible way to investigate relationships between snow cover and vegetation and their interactions under complex terrain (i.e.,  $\leq 500$  m) and micro-climate conditions [79–81]. The cloud cover, temporal resolution, and other production processes may also induce the NDVI product uncertainties [49].

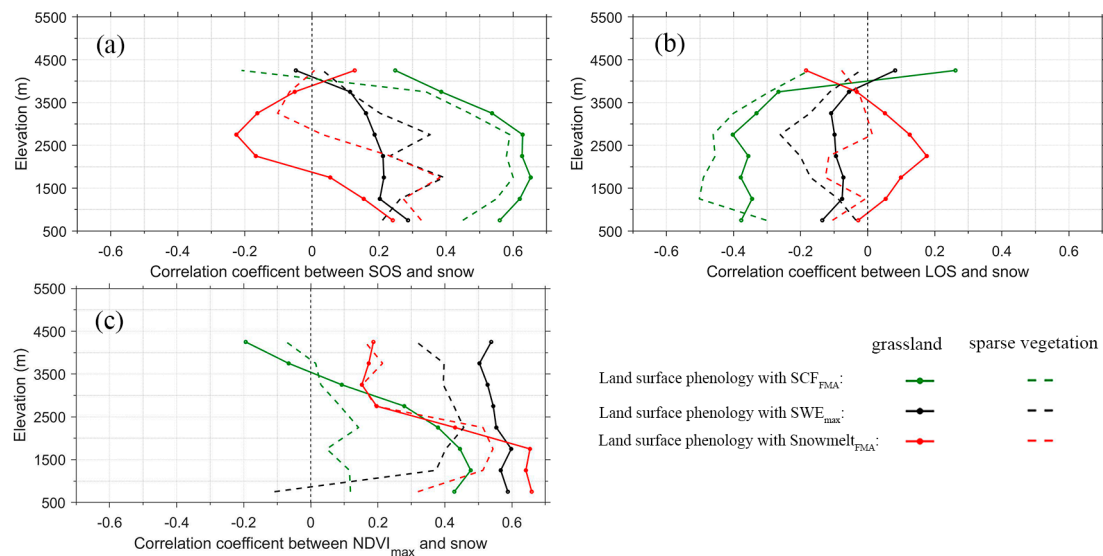


**Figure 8.** Elevation variation of correlation coefficients between (a) SOS, (b) LOS, and (c)  $NDVI_{max}$  and  $SCF_{FMA}$ ,  $SWE_{max}$ , and  $Snowmelt_{FMA}$  for grassland and sparse vegetation.

The dynamic threshold is a simple and efficient method to derive the land surface phenology in existing studies [57,58], but the lack of in situ observations to validate its performance increased the uncertainty of land surface phenology calculation in this study. Land cover experienced a dramatic change with a rapid increase in crop area around the TS during the past decades [82]; vegetation types based on the fixed CCI-LC 2000 map might not accurately reflect the land cover changes and their phenology. For example, large proportions of crop area were converted from grassland or sparse vegetation around the TS [83], which may increase the greenness and advance the SOS. Meanwhile, previous studies reported that the expansion of irrigated areas could affect the mountainous climate by increasing precipitation and reducing the temperature, and then modifying the regional snow status [84,85]. Similarly, the glacier areas are significantly shrinking due to climate warming, which increased glacier/snow melt water and benefited vegetation greening [71].

## 5. Conclusions

This study investigated the variability of land surface phenology metrics and their responses to the snow dynamics in the Tianshan Mountains from 1983 to 2015 using the GIMMS NDVI product and a snow dataset from a regional climate model dynamic downscaling simulation. The main findings of this study include the following:

- 1 The annual mean start of growing season was 106.30 (day of the year) and exhibited a significant decrease trend ( $p < 0.05$ ,  $-2.45$  days/decade), which concentrated in the Ili Valley and Western Tianshan Mountains with an elevation from 2500 to 3500 m a.s.l. In contrast, the length of growing season was 162.24 days and exhibited a significant increase trend ( $p < 0.05$ ,  $2.98$  days/decade), which was mainly seen in low-elevation regions (elevations below 3000 m a.s.l.) of the Ili Valley and Western Tianshan Mountains.
- 2 Snow cover fraction during February–April has a significant positive effect on the start of growing season. In contrast, snowmelt amount during February–April and annual maximum snow water equivalent have an almost equally significant positive correlation with  $NDVI_{max}$ . In particular, the start of growing season of grassland was the most sensitive to variations of snow cover fraction during February–April than that of other vegetation types, and their strong relationship was mainly located at elevations from 1500 to 3000 m a.s.l. In addition, its greenness was significantly affected by the annual maximum snow water equivalent in all elevation bands.

- 3 Both decreased snow cover fraction and increased temperature in the early spring period caused the significant advance of the start date of vegetation growing season, consequently prolonging the length of vegetation growing season. Large annual maximum snow water equivalent and more snowmelt amount could significantly promote the increase in NDVI<sub>max</sub> by consistently regulating the soil moisture.

The variability of large-scale atmospheric circulations, such as El Nino and Atlantic multi-decadal oscillation (AMO), could significantly impact regional temperature and precipitation [86,87], and their relations with snow and vegetation need to be investigated further. Notably, although the significantly advanced SOS was found in the Tianshan Mountains and snow variability plays a critical role, it is necessary to quantify the contribution of snow, temperature, and precipitation to the change in the early spring vegetation growth. Meanwhile, the relationships between the spring land surface phenology and elevation-dependent warming should be considered using a finer resolution product in the next work.

**Author Contributions:** T.Y.: Writing—Original Draft, Methodology Software; Q.L.: Writing—Review & Editing; Q.Z.: funding acquisition; R.H.: Writing—Review & Editing; F.C.: Visualization; L.L.: Writing—Review & Editing, supervision, Project administration. All authors have read and agreed to the published version of the manuscript.

**Funding:** This study was supported by the Strategic Priority Research Program of Chinese Academy of Sciences (No. XDA23090303), the project of Applications for network security and informatization, CAS (No. CAS-WX2021SF-010604), the projects of the Second Tibetan Plateau Scientific Expedition and Research Program (STEP) (No. 2019QZKK0902), the Pan-Third Pole Environment Study for a Green Silk Road (Pan-TPE) (No. XDA2004030202), and the China Postdoctoral Science Foundation Funded Project (No. 2021M703132).

**Conflicts of Interest:** The authors declare no conflict of interest.

## References

1. Miguez-Macho, G.; Fan, Y. Spatiotemporal origin of soil water taken up by vegetation. *Nature* **2021**, *598*, 624–628. [[CrossRef](#)] [[PubMed](#)]
2. Piao, S.; Wang, X.; Park, T.; Chen, C.; Lian, X.; He, Y.; Bjerke, J.W.; Chen, A.; Ciais, P.; Tømmervik, H.; et al. Characteristics, drivers and feedbacks of global greening. *Nat. Rev. Earth Environ.* **2020**, *1*, 14–27. [[CrossRef](#)]
3. Forzieri, G.; Miralles, D.G.; Ciais, P.; Alkama, R.; Ryu, Y.; Duveiller, G.; Zhang, K.; Robertson, E.; Kautz, M.; Martens, B.; et al. Increased control of vegetation on global terrestrial energy fluxes. *Nat. Clim. Chang.* **2020**, *10*, 356–362. [[CrossRef](#)]
4. Richardson, A.D.; Keenan, T.F.; Migliavacca, M.; Ryu, Y.; Sonnentag, O.; Toomey, M. Climate change, phenology, and phenological control of vegetation feedbacks to the climate system. *Agric. For. Meteorol.* **2013**, *169*, 156–173. [[CrossRef](#)]
5. Gao, M.; Piao, S.; Chen, A.; Yang, H.; Liu, Q.; Fu, Y.H.; Janssens, I.A. Divergent changes in the elevational gradient of vegetation activities over the last 30 years. *Nat. Commun.* **2019**, *10*, 2970. [[CrossRef](#)]
6. Immerzeel, W.W.; Lutz, A.F.; Andrade, M.; Bahl, A.; Biemans, H.; Bolch, T.; Hyde, S.; Brumby, S.; Davies, B.J.; Elmore, A.C.; et al. Importance and vulnerability of the world's water towers. *Nature* **2020**, *577*, 364–369. [[CrossRef](#)]
7. Pepin, N.C.; Arnone, E.; Gobiet, A.; Haslinger, K.; Kotlarski, S.; Notarnicola, C.; Palazzi, E.; Seibert, P.; Serafin, S.; Schöner, W.; et al. Climate Changes and Their Elevational Patterns in the Mountains of the World. *Rev. Geophys.* **2022**, *60*, e2020RG000730. [[CrossRef](#)]
8. Xu, L.; Myneni, R.B.; Chapin, F.S.; Callaghan, T.V.; Pinzon, J.E.; Tucker, C.J.; Zhu, Z.; Bi, J.; Ciais, P.; Tømmervik, H.; et al. Temperature and vegetation seasonality diminishment over northern lands. *Nat. Clim. Chang.* **2013**, *3*, 581–586. [[CrossRef](#)]
9. Zhu, Z.; Piao, S.; Myneni, R.B.; Huang, M.; Zeng, Z.; Canadell, J.G.; Ciais, P.; Sitch, S.; Friedlingstein, P.; Arneeth, A.; et al. Greening of the Earth and its drivers. *Nat. Clim. Chang.* **2016**, *6*, 791–795. [[CrossRef](#)]
10. Cleverly, J.; Eamus, D.; Restrepo Coupe, N.; Chen, C.; Maes, W.; Li, L.; Faux, R.; Santini, N.S.; Rumman, R.; Yu, Q.; et al. Soil moisture controls on phenology and productivity in a semi-arid critical zone. *Sci. Total Environ.* **2016**, *568*, 1227–1237. [[CrossRef](#)]
11. Ren, S.; Chen, X.; Lang, W.; Schwartz, M.D. Climatic Controls of the Spatial Patterns of Vegetation Phenology in Midlatitude Grasslands of the Northern Hemisphere. *J. Geophys. Res. Biogeosci.* **2018**, *123*, 2323–2336. [[CrossRef](#)]
12. Piao, S.; Liu, Q.; Chen, A.; Janssens, I.A.; Fu, Y.; Dai, J.; Liu, L.; Lian, X.; Shen, M.; Zhu, X. Plant phenology and global climate change: Current progresses and challenges. *Glob. Chang. Biol.* **2019**, *25*, 1922–1940. [[CrossRef](#)]
13. Yang, B.; He, M.; Shishov, V.; Tychkov, I.; Vaganov, E.; Rossi, S. New perspective on spring vegetation phenology and global climate change based on Tibetan Plateau tree-ring data. *Proc. Natl. Acad. Sci. USA* **2017**, *114*, 6966–6971. [[CrossRef](#)]

14. Gavrilov, M.B.; An, W.; Xu, C.; Radaković, M.G.; Hao, Q.; Yang, F.; Guo, Z.; Perić, Z.; Gavrilov, G.; Marković, S.B. Independent aridity and drought pieces of evidence based on meteorological data and tree ring data in Southeast Banat, Vojvodina, Serbia. *Atmosphere* **2019**, *10*, 586. [[CrossRef](#)]
15. Huang, K.; Zhang, Y.; Tagesson, T.; Brandt, M.; Wang, L.; Chen, N.; Zu, J.; Jin, H.; Cai, Z.; Tong, X.; et al. The confounding effect of snow cover on assessing spring phenology from space: A new look at trends on the Tibetan Plateau. *Sci. Total Environ.* **2021**, *756*, 144011. [[CrossRef](#)]
16. Xie, J.; Kneubühler, M.; Garonna, I.; de Jong, R.; Notarnicola, C.; De Gregorio, L.; Schaepman, M.E. Relative Influence of Timing and Accumulation of Snow on Alpine Land Surface Phenology. *J. Geophys. Res. Biogeosci.* **2018**, *123*, 561–576. [[CrossRef](#)]
17. Tomaszewska, M.A.; Nguyen, L.H.; Henebry, G.M. Land surface phenology in the highland pastures of montane Central Asia: Interactions with snow cover seasonality and terrain characteristics. *Remote Sens. Environ.* **2020**, *240*, 111675. [[CrossRef](#)]
18. Yun, J.; Jeong, S.J.; Ho, C.H.; Park, C.E.; Park, H.; Kim, J. Influence of winter precipitation on spring phenology in boreal forests. *Glob. Chang. Biol.* **2018**, *24*, 5176–5187. [[CrossRef](#)]
19. Chen, X.; Yang, Y. Observed earlier start of the growing season from middle to high latitudes across the Northern Hemisphere snow-covered landmass for the period 2001–2014. *Environ. Res. Lett.* **2020**, *15*, 034042. [[CrossRef](#)]
20. Xie, J.; Hüsler, F.; de Jong, R.; Chimani, B.; Asam, S.; Sun, Y.; Schaepman, M.E.; Kneubühler, M. Spring Temperature and Snow Cover Climatology Drive the Advanced Springtime Phenology (1991–2014) in the European Alps. *J. Geophys. Res. Biogeosci.* **2021**, *126*, e2020JG006150. [[CrossRef](#)]
21. Zheng, J.; Jia, G.; Xu, X. Agricultural and Forest Meteorology Earlier snowmelt predominates advanced spring vegetation greenup in Alaska. *Agric. For. Meteorol.* **2022**, *315*, 108828. [[CrossRef](#)]
22. Henderson, G.R.; Peings, Y.; Furtado, J.C.; Kushner, P.J. Snow–atmosphere coupling in the Northern Hemisphere. *Nat. Clim. Chang.* **2018**, *8*, 954–963. [[CrossRef](#)]
23. Barnett, T.P.; Adam, J.C.; Lettenmaier, D.P. Potential impacts of a warming climate on water availability in snow-dominated regions. *Nature* **2005**, *438*, 303–309. [[CrossRef](#)]
24. Kraaijenbrink, P.D.A.; Stigter, E.E.; Yao, T.; Immerzeel, W.W. Climate change decisive for Asia’s snow meltwater supply. *Nat. Clim. Chang.* **2021**, *11*, 591–597. [[CrossRef](#)]
25. Zhang, T. Influence of the seasonal snow cover on the ground thermal regime: An overview. *Rev. Geophys.* **2005**, *43*, RG4002. [[CrossRef](#)]
26. Pulliainen, J.; Aurela, M.; Laurila, T.; Aalto, T.; Takala, M.; Salminen, M.; Kulmala, M.; Barr, A.; Heimann, M.; Lindroth, A.; et al. Early snowmelt significantly enhances boreal springtime carbon uptake. *Proc. Natl. Acad. Sci. USA.* **2017**, *114*, 11081–11086. [[CrossRef](#)]
27. Peng, S.; Piao, S.; CIAIS, P.; Fang, J.; Wang, X. Change in winter snow depth and its impacts on vegetation in China. *Glob. Chang. Biol.* **2010**, *16*, 3004–3013. [[CrossRef](#)]
28. Wang, X.; Wang, T.; Guo, H.; Liu, D.; Zhao, Y.; Zhang, T.; Liu, Q.; Piao, S. Disentangling the mechanisms behind winter snow impact on vegetation activity in northern ecosystems. *Glob. Chang. Biol.* **2018**, *24*, 1651–1662. [[CrossRef](#)]
29. Jinfei, Y.; Xiaobing, Z.; Benfeng, Y.; Yonggang, L.; Yuanming, Z. Species-dependent responses of root growth of herbaceous plants to snow cover changes in a temperate desert, Northwest China. *Plant Soil* **2021**, *459*, 249–260. [[CrossRef](#)]
30. Evan, A.; Eisenman, I. A mechanism for regional variations in snowpack melt under rising temperature. *Nat. Clim. Chang.* **2021**, *11*, 326–330. [[CrossRef](#)]
31. Notarnicola, C. Hotspots of snow cover changes in global mountain regions over 2000–2018. *Remote Sens. Environ.* **2020**, *243*, 111781. [[CrossRef](#)]
32. Chen, Y.; Li, Z.; Fang, G.; Li, W. Large Hydrological Processes Changes in the Transboundary Rivers of Central Asia. *J. Geophys. Res. Atmos.* **2018**, *123*, 5059–5069. [[CrossRef](#)]
33. Farinotti, D.; Longuevergne, L.; Moholdt, G.; Duethmann, D.; Mölg, T.; Bolch, T.; Vorogushyn, S.; Güntner, A. Substantial glacier mass loss in the Tien Shan over the past 50 years. *Nat. Geosci.* **2015**, *8*, 716–722. [[CrossRef](#)]
34. Hu, Z.; Zhang, C.; Hu, Q.; Tian, H. Temperature changes in central Asia from 1979 to 2011 based on multiple datasets. *J. Clim.* **2014**, *27*, 1143–1167. [[CrossRef](#)]
35. Yang, T.; Li, Q.; Ahmad, S.; Zhou, H.; Li, L. Changes in snow phenology from 1979 to 2016 over the Tianshan Mountains, Central Asia. *Remote Sens.* **2019**, *11*, 499. [[CrossRef](#)]
36. Li, Q.; Yang, T.; Zhou, H.; Li, L. Patterns in snow depth maximum and snow cover days during 1961–2015 period in the Tianshan Mountains, Central Asia. *Atmos. Res.* **2019**, *228*, 14–22. [[CrossRef](#)]
37. Yang, T.; Li, Q.; Chen, X.; Hamdi, R.; De Maeyer, P.; Li, L. Variation of Snow Mass in a Regional Climate Model Downscaling Simulation Covering the Tianshan Mountains, Central Asia. *J. Geophys. Res. Atmos.* **2021**, *126*, e2020JD034183. [[CrossRef](#)]
38. Li, Y.; Chen, Y.; Sun, F.; Li, Z. Recent vegetation browning and its drivers on Tianshan Mountain, Central Asia. *Ecol. Indic.* **2021**, *129*, 107912. [[CrossRef](#)]
39. Li, Z.; Chen, Y.; Li, W.; Deng, H.; Fang, G. Potential impacts of climate change on vegetation dynamics in Central Asia. *J. Geophys. Res. Atmos.* **2015**, *120*, 12345–12356. [[CrossRef](#)]
40. Jiang, L.; Jiapaer, G.; Bao, A.; Guo, H.; Ndayisaba, F. Vegetation dynamics and responses to climate change and human activities in Central Asia. *Sci. Total Environ.* **2017**, *599–600*, 967–980. [[CrossRef](#)]

41. Wu, L.; Ma, X.; Dou, X.; Zhu, J.; Zhao, C. Impacts of climate change on vegetation phenology and net primary productivity in arid Central Asia. *Sci. Total Environ.* **2021**, *796*, 149055. [[CrossRef](#)]
42. Zhang, B.; Li, X.; Li, C.; Nyiransengiyumva, C.; Qin, Q. Alpine vegetation responses to snow phenology in the Chinese Tianshan mountainous region. *J. Mt. Sci.* **2022**, *19*, 1307–1323. [[CrossRef](#)]
43. Dong, C. Remote sensing, hydrological modeling and in situ observations in snow cover research: A review. *J. Hydrol.* **2018**, *561*, 573–583. [[CrossRef](#)]
44. Sorg, A.; Bolch, T.; Stoffel, M.; Solomina, O.; Beniston, M. Climate change impacts on glaciers and runoff in Tien Shan (Central Asia). *Nat. Clim. Chang.* **2012**, *2*, 725–731. [[CrossRef](#)]
45. Lu, X.; Tang, G.; Wang, X.; Liu, Y.; Jia, L.; Xie, G.; Li, S.; Zhang, Y. Correcting GPM IMERG precipitation data over the Tianshan Mountains in China. *J. Hydrol.* **2019**, *575*, 1239–1252. [[CrossRef](#)]
46. Aizen, V.B.; Kuzmichenok, V.A.; Surazakov, A.B.; Aizen, E.M. Glacier changes in the Tien Shan as determined from topographic and remotely sensed data. *Glob. Planet. Chang.* **2007**, *56*, 328–340. [[CrossRef](#)]
47. Yang, T.; Li, Q.; Hamdi, R.; Zou, Q.; Chen, X.; De Maeyer, P.; Cui, F.; Li, L. Snowfall climatology in the Tianshan Mountains based on 36 cold seasons of WRF dynamical downscaling simulation. *Atmos. Res.* **2022**, *270*, 106057. [[CrossRef](#)]
48. Pinzon, J.E.; Tucker, C.J. A non-stationary 1981–2012 AVHRR NDVI3g time series. *Remote Sens.* **2014**, *6*, 6929–6960. [[CrossRef](#)]
49. Tian, F.; Fensholt, R.; Verbesselt, J.; Grogan, K.; Horion, S.; Wang, Y. Evaluating temporal consistency of long-term global NDVI datasets for trend analysis. *Remote Sens. Environ.* **2015**, *163*, 326–340. [[CrossRef](#)]
50. ESA. Land Cover CCI Product User Guide Version 2. Technical Report. 2017. Available online: [maps.elie.ucl.ac.be/CCI/viewer/download/ESACCI-LC-Ph2-PUGv2\\_2.0.pdf](https://maps.elie.ucl.ac.be/CCI/viewer/download/ESACCI-LC-Ph2-PUGv2_2.0.pdf) (accessed on 20 February 2020).
51. Yang, Y.; Xiao, P.; Feng, X.; Li, H. Accuracy assessment of seven global land cover datasets over China. *ISPRS J. Photogramm. Remote Sens.* **2017**, *125*, 156–173. [[CrossRef](#)]
52. Skamarock, W.C.; Klemp, J.B. A time-split nonhydrostatic atmospheric model for weather research and forecasting applications. *J. Comput. Phys.* **2008**, *227*, 3465–3485. [[CrossRef](#)]
53. Niu, G.Y.; Yang, Z.L.; Mitchell, K.E.; Chen, F.; Ek, M.B.; Barlage, M.; Kumar, A.; Manning, K.; Niyogi, D.; Rosero, E.; et al. The community Noah land surface model with multiparameterization options (Noah-MP): 1. Model description and evaluation with local-scale measurements. *J. Geophys. Res. Atmos.* **2011**, *116*, D12109. [[CrossRef](#)]
54. Zeng, L.; Wardlaw, B.D.; Xiang, D.; Hu, S.; Li, D. A review of vegetation phenological metrics extraction using time-series, multispectral satellite data. *Remote Sens. Environ.* **2020**, *237*, 111511. [[CrossRef](#)]
55. Liu, X.; Chen, Y.; Li, Z.; Li, Y.; Zhang, Q.; Zan, M. Driving forces of the changes in vegetation phenology in the qinghai-tibet plateau. *Remote Sens.* **2021**, *13*, 4952. [[CrossRef](#)]
56. Yu, H.; Luedeling, E.; Xu, J. Winter and spring warming result in delayed spring phenology on the Tibetan Plateau. *Proc. Natl. Acad. Sci. USA* **2010**, *107*, 22151–22156. [[CrossRef](#)]
57. Zhang, Q.; Kong, D.; Shi, P.; Singh, V.P.; Sun, P. Vegetation phenology on the Qinghai-Tibetan Plateau and its response to climate change (1982–2013). *Agric. For. Meteorol.* **2018**, *248*, 408–417. [[CrossRef](#)]
58. White, M.A.; de Beurs, K.M.; Didan, K.; Inouye, D.W.; Richardson, A.D.; Jensen, O.P.; O’Keefe, J.; Zhang, G.; Nemani, R.R.; van Leeuwen, W.J.D.; et al. Intercomparison, interpretation, and assessment of spring phenology in North America estimated from remote sensing for 1982–2006. *Glob. Chang. Biol.* **2009**, *15*, 2335–2359. [[CrossRef](#)]
59. Chen, J.; Jönsson, P.; Tamura, M.; Gu, Z.; Matsushita, B.; Eklundh, L. A simple method for reconstructing a high-quality NDVI time-series data set based on the Savitzky-Golay filter. *Remote Sens. Environ.* **2004**, *91*, 332–344. [[CrossRef](#)]
60. Wang, X.; Xiao, J.; Li, X.; Cheng, G.; Ma, M.; Zhu, G.; Altaf Arain, M.; Andrew Black, T.; Jassal, R.S. No trends in spring and autumn phenology during the global warming hiatus. *Nat. Commun.* **2019**, *10*, 2389. [[CrossRef](#)]
61. Sen, P.K. Journal of the American Statistical Estimates of the Regression Coefficient Based on Kendall’s Tau. *J. Am. Stat. Assoc.* **1968**, *63*, 1379–1389. [[CrossRef](#)]
62. Mann, H.B. Nonparametric tests against trend. *Econometrica* **1945**, *13*, 245–259. [[CrossRef](#)]
63. Kendall, M.G. *Rank Correlation Methods*; Griffin: London, UK, 1975.
64. Qi, Y.; Wang, H.; Ma, X.; Zhang, J.; Yang, R. Relationship between vegetation phenology and snow cover changes during 2001–2018 in the Qilian Mountains. *Ecol. Indic.* **2021**, *133*, 108351. [[CrossRef](#)]
65. Kelsey, K.C.; Pedersen, S.H.; Leffler, A.J.; Sexton, J.O.; Feng, M.; Welker, J.M. Winter snow and spring temperature have differential effects on vegetation phenology and productivity across Arctic plant communities. *Glob. Chang. Biol.* **2021**, *27*, 1572–1586. [[CrossRef](#)]
66. Wang, T.; Peng, S.; Lin, X.; Chang, J. Declining snow cover may affect spring phenological trend on the Tibetan Plateau. *Proc. Natl. Acad. Sci. USA* **2013**, *110*, E2854–E2855. [[CrossRef](#)]
67. Rumpf, S.B.; Gravey, M.; Brönnimann, O.; Luoto, M.; Cianfrani, C.; Mariethoz, G.; Guisan, A. vegetation productivity in the European Alps. *Science* **2022**, *1122*, 1119–1122. [[CrossRef](#)]
68. Déry, S.J.; Brown, R.D. Recent Northern Hemisphere snow cover extent trends and implications for the snow-albedo feedback. *Geophys. Res. Lett.* **2007**, *34*, 2–7. [[CrossRef](#)]
69. Wang, X.; Wu, C.; Peng, D.; Gonsamo, A.; Liu, Z. Snow cover phenology affects alpine vegetation growth dynamics on the Tibetan Plateau: Satellite observed evidence, impacts of different biomes, and climate drivers. *Agric. For. Meteorol.* **2018**, *256–257*, 61–74. [[CrossRef](#)]

70. Wang, K.; Zhang, L.; Qiu, Y.; Ji, L.; Tian, F.; Wang, C.; Wang, Z. Snow effects on alpine vegetation in the Qinghai-Tibetan Plateau. *Int. J. Digit. Earth* **2015**, *8*, 56–73. [[CrossRef](#)]
71. Zheng, L.; Xu, J.; Li, D.; Xia, Z.; Chen, Y.; Xu, G.; Lu, D. Increasing control of climate warming on the greening of alpine pastures in central Asia. *Int. J. Appl. Earth Obs. Geoinf.* **2021**, *105*, 102606. [[CrossRef](#)]
72. Körner, C.; Paulsen, J. A world-wide study of high altitude treeline temperatures. *J. Biogeogr.* **2004**, *31*, 713–732. [[CrossRef](#)]
73. Thompson, J.A.; Paull, D.J.; Lees, B.G. Using phase-spaces to characterize land surface phenology in a seasonally snow-covered landscape. *Remote Sens. Environ.* **2015**, *166*, 178–190. [[CrossRef](#)]
74. Terzago, S.; Andreoli, V.; Arduini, G.; Balsamo, G.; Campo, L.; Cassardo, C.; Cremonese, E.; Dolia, D.; Gabellani, S.; Von Hardenberg, J.; et al. Sensitivity of snow models to the accuracy of meteorological forcings in mountain environments. *Hydrol. Earth Syst. Sci.* **2020**, *24*, 4061–4090. [[CrossRef](#)]
75. Wrzesien, M.L.; Pavelsky, T.M.; Durand, M.T.; Dozier, J.; Lundquist, J.D. Characterizing Biases in Mountain Snow Accumulation From Global Data Sets. *Water Resour. Res.* **2019**, *55*, 9873–9891. [[CrossRef](#)]
76. Bonekamp, P.N.J.; Collier, E.; Immerzeel, W. The Impact of spatial resolution, land use, and spinup time on resolving spatial precipitation patterns in the Himalayas. *J. Hydrometeorol.* **2018**, *19*, 1565–1581. [[CrossRef](#)]
77. Yang, T.; Li, Q.; Chen, X.; Hamdi, R.; De Maeyer, P.; Kurban, A.; Li, L. Improving snow simulation with more realistic vegetation parameters in a regional climate model in the Tianshan Mountains, Central Asia. *J. Hydrol.* **2020**, *590*, 125525. [[CrossRef](#)]
78. Guay, K.C.; Beck, P.S.A.; Berner, L.T.; Goetz, S.J.; Baccini, A.; Buermann, W. Vegetation productivity patterns at high northern latitudes: A multi-sensor satellite data assessment. *Glob. Chang. Biol.* **2014**, *20*, 3147–3158. [[CrossRef](#)]
79. Vrieling, A.; Meroni, M.; Darvishzadeh, R.; Skidmore, A.K.; Wang, T.; Zurita-Milla, R.; Oosterbeek, K.; O'Connor, B.; Paganini, M. Vegetation phenology from Sentinel-2 and field cameras for a Dutch barrier island. *Remote Sens. Environ.* **2018**, *215*, 517–529. [[CrossRef](#)]
80. Yan, D.; Scott, R.L.; Moore, D.J.P.; Biederman, J.A.; Smith, W.K. Understanding the relationship between vegetation greenness and productivity across dryland ecosystems through the integration of PhenoCam, satellite, and eddy covariance data. *Remote Sens. Environ.* **2019**, *223*, 50–62. [[CrossRef](#)]
81. Tian, F.; Cai, Z.; Jin, H.; Hufkens, K.; Scheifinger, H.; Tagesson, T.; Smets, B.; Van Hoolst, R.; Bonte, K.; Ivits, E.; et al. Calibrating vegetation phenology from Sentinel-2 using eddy covariance, PhenoCam, and PEP725 networks across Europe. *Remote Sens. Environ.* **2021**, *260*, 112456. [[CrossRef](#)]
82. Zhang, M.; Luo, G.; Cao, X.; Hamdi, R.; Li, T.; Cai, P.; Ye, H.; He, H. Numerical Simulation of the Irrigation Effects on Surface Fluxes and Local Climate in Typical Mountain-Oasis-Desert Systems in the Central Asia Arid Area. *J. Geophys. Res. Atmos.* **2019**, *124*, 12485–12506. [[CrossRef](#)]
83. Wei, H.; Xiong, L.; Tang, G.; Strobl, J.; Xue, K. Spatial—Temporal variation of land use and land cover change in the glacial affected area of the Tianshan Mountains. *Catena* **2021**, *202*, 105256. [[CrossRef](#)]
84. Cai, P.; Hamdi, R.; Luo, G.; He, H.; Zhang, M.; Termonia, P.; De Maeyer, P. Agriculture intensification increases summer precipitation in Tianshan Mountains, China. *Atmos. Res.* **2019**, *227*, 140–146. [[CrossRef](#)]
85. de Kok, R.J.; Kraaijenbrink, P.D.A.; Tuinenburg, O.A.; Bonekamp, P.N.J.; Immerzeel, W.W. Towards understanding the pattern of glacier mass balances in High Mountain Asia using regional climatic modelling. *Cryosphere* **2020**, *14*, 3215–3234. [[CrossRef](#)]
86. Yang, T.; Li, Q.; Chen, X.; De Maeyer, P.; Yan, X.; Liu, Y.; Zhao, T.; Li, L. Spatiotemporal variability of the precipitation concentration and diversity in Central Asia. *Atmos. Res.* **2020**, *241*, 104954. [[CrossRef](#)]
87. Gerlitz, L.; Steirou, E.; Schneider, C.; Moron, V.; Vorogushyn, S.; Merz, B. Variability of the cold season climate in central asia. Part I: Weather types and their tropical and extratropical drivers. *J. Clim.* **2018**, *31*, 7185–7207. [[CrossRef](#)]